Anisotropic spin dynamics in the frustrated chain $Ca_3Co_2O_6$ detected by single-crystal ^{59}Co NMR

Yasuhiro Shimizu,[1,2] Munehisa Horibe,[1] Hiroshi Nanba,[1] Tsuyoshi Takami,[1] and Masayuki Itoh[1]
[1]*Department of Physics, Graduate School of Science, Nagoya University, Furo-cho, Chikusa-ku, Nagoya 464-8602, Japan*
[2]*Institute for Advanced Research, Nagoya University, Furo-cho, Chikusa-ku, Nagoya 464-8601, Japan*
(Received 20 April 2010; revised manuscript received 25 August 2010; published 17 September 2010)

Static and dynamic magnetic properties are investigated by ^{59}Co NMR measurements on a single crystal of $Ca_3Co_2O_6$, a rare model of the ferromagnetic Ising chain coupled antiferromagnetically on a triangular lattice. Above a ferrimagnetic order transition temperature $T_N=25$ K, the static spin susceptibility probed by the ^{59}Co Knight shift shows anisotropic behavior in the temperature dependence, consistent with ferromagnetic interactions along the *c*-axis chain and antiferromagnetic interactions in the *ab* plane. Correspondingly, the dynamical spin susceptibility obtained from the ^{59}Co nuclear spin-lattice relaxation rate is also highly anisotropic. The intrachain ferromagnetic correlation steeply develops below 300 K while the interchain antiferromagnetic one does below 120 K with the critical exponent expected in the two-dimensional Ising antiferromagnet. Below T_N, the low-energy excitation arising from the predominant spin-wave magnons has an anisotropic full gap, reflecting the strongly Ising nature. Clear microscopic evidence of the ferrimagnetic order is demonstrated in the ^{59}Co NMR spectra at 5 K. Rotation of the external magnetic field from the *ab* plane to the *c* axis shows the first-order transition from the ferrimagnetic to the fully polarized state. The ferrimagnetic state with the uniform magnitude of magnetic moment is observed even in the transverse field adjusted parallel to the *ab* plane.

DOI: 10.1103/PhysRevB.82.094430 PACS number(s): 76.60.−k, 75.40.Gb, 75.50.Ee, 75.30.−m

I. INTRODUCTION

Low-dimensional and frustrated antiferromagnets with spin $S>1$ have been extensively studied as models of critical phenomena of semiclassical phase transitions.[1–3] Since the proposal of the Kosterlitz-Thouless-type transition on a triangular lattice antiferromagnet (TLA),[4] the critical dynamics classified into new universality class has attracted much attention on the classical Heisenberg or XY TLA. Many experimental results with the easy-plane anisotropy on the TLA such as ABX_3,[3] VCl_2,[5] $BaNi_2V_2O_8$,[6] and delafossites[7] were discussed along with the scenario of the Z_2 vortex order. In contrast, few examples have been investigated for the classical Ising TLA with the easy-axis anisotropy, as well as the quantum ($S=1/2$) one recently highlighted in the emergent E_8 symmetry.[8] $Ca_3Co_2O_6$ (Refs. 9 and 10) and its analogs $A_3MM'O_6$ (A=alkaline-earth metal; M,M'=transition metals) (Refs. 11–15) are the Ising TLA having ferromagnetic one-dimensional (1D) chains arranged on the triangular lattice. The series of materials exhibit various ground states such as partially disordered antiferromagnetic (PDA),[12] ferrimagnetic[13] and possible spin-liquid states, and have potential multiferroic[14] and thermoelectric[15] applications.

$Ca_3Co_2O_6$ is the highlight compound of the anomalous PDA state and the devil's staircase transition under magnetic field. The 1D chain of $Ca_3Co_2O_6$ consists of alternating stacks of the face-sharing CoO_6 octahedra and trigonal prisms along the *c* axis.[16] A difference in crystal field at two kinds of trivalent Co ions gives the low-spin ($S=0$) Co1 for the octahedron and the high-spin ($S=2$) Co2 for the trigonal prism. The magnetic interaction between Co2 mediated via Co1 along the *c* axis is ferromagnetic, as seen in the strongly enhanced magnetic susceptibility,[10,17] although the origin is theoretically nontrivial and some models have been proposed.[16–18] The chains are located on the corner of the triangular lattice in the *ab* plane with the staggered interchain Co2 configuration, which construct helical antiferromagnetic paths.

In the absence of external magnetic field, a second-order phase transition takes place at $T_N=25$ K, which becomes a crossover with increasing the magnetic field.[19] The neutron-scattering and μSR measurements suggested a PDA state,[20–22] analogous to the Ising TLA system such as Ca_3CoRhO_6 (Ref. 12) and $CsCoCl_3$.[23] However, the neutron-scattering[24] and the resonant x-ray scattering[25] experiments recently revealed an incommensurate moment distribution with a long period along the *c* axis, which was interpreted as a competition between 1D ferromagnetic and helical antiferromagnetic interactions.[26] The long-period incommensurate structure may be the 1D Ising version of the skymion lattice arising from the competing ferromagnetic-antiferromagnetic interactions in the two-dimensional (2D) XY system.[27]

Application of a weak magnetic field along the *c* axis induces uniform magnetic moments within the chain, constructing the up-up-down ferrimagnetic structure in the *ab* plane, as observed in a magnetization plateau at 1/3 of the saturated moment below 25 K.[9,10,28,29] The 2D ferrimagnetic structure was proposed to be incommensurate with slow dynamics due to the remaining frustration,[30–33] which was manifested in frequency dependence of the ac magnetic susceptibility below T_N.[34] The magnetization plateau becomes more complex below 4 K,[29] with the final step around 4 T above which the moments are fully polarized to the external magnetic field with a saturated value of ~4.7 μ_B.[17] The magnitude of the moment is somewhat larger than that expected in $S=2$, which is attributed to the significant orbital moment arising from degenerated multiplets of Co2.[35] Al-

though the μSR measurement reported the onset of antiferromagnetic fluctuations below 100 K,[36] the previous NMR (Ref. 37) and neutron-scattering[24] measurements in $Ca_3Co_2O_6$ have been limited only below T_N. Sampathkumaran *et al.*[37] observed a ^{59}Co NMR signal below 12 K and measured the brief temperature (T) dependence of the nuclear spin-lattice relaxation rate $1/T_1$ and the spin-echo decay rate $1/T_2$, which was interpreted as the spin freezing at low temperatures. Furthermore, the observed broad NMR spectra in a powder sample could not evidence the ferrimagnetic state. Thus the previous experimental and theoretical studies have been focused on the low-temperature magnetic order, and the statistical and microscopic nature of the phase transition is less understood.

In this paper, we report detailed ^{59}Co NMR measurements first conducted on a single crystal of $Ca_3Co_2O_6$. Using a short rf pulse and an interval time between first and second pulses, we could succeed to measure the ^{59}Co Knight shift K and $1/T_1$ on the Co1 site in the paramagnetic state. Owing to the axially symmetric crystal, the intrachain ferromagnetic and interchain antiferromagnetic correlations are separately obtained, which allows to determining the initial critical exponent of the dynamical spin correlation. The obtained static and dynamical susceptibilities exhibit strong Ising behavior. The ^{59}Co NMR spectra clearly show the static magnetic order below T_N, which is also confirmed by gapped excitations as usually observed in anisotropic antiferromagnets. Finally, a field-induced transition will be shown under the external magnetic field rotated from the *ab* plane to the *c* axis.

II. EXPERIMENTAL PROCEDURE

Single crystals of $Ca_3Co_2O_6$ were grown by a flux method at 980 °C by using $Ca_3Co_4O_9$ and K_2CO_3.[38] Magnetic susceptibility was measured for the aligned single crystals to obtain the sufficient signal-to-noise ratio by using a superconducting quantum interference device magnetometer [Quantum Design, magnetic property measurement system (MPMS)-7] in the field-cooling process at 7.0 T. ^{59}Co NMR measurements were performed on a single crystal in a temperature range, 2–300 K, under a fixed magnetic field, H_0 =9.4026 T. Frequency-swept NMR spectra were obtained by Fourier transformation of spin-echo signals with the $\pi/2$ pulse width of 1 μs and the interval time τ=6 μs between the first and second pulses. K was determined as the relative shift from the bare resonance frequency $\nu_0 = {}^{59}\gamma H_0/2\pi$ =94.534 MHz, where $^{59}\gamma = 2\pi \times 10.054$ MHz/T is the ^{59}Co nuclear gyromagnetic ratio. The ^{59}Co NMR spectrum was split into equally spaced seven lines due to the nuclear quadrupole interaction of nuclear spin $I=7/2$. The nuclear spin-lattice relaxation rate $1/T_1$ was obtained for the nuclear magnetization recovery of the central resonance line after an inversion pulse.

III. EXPERIMENTAL RESULTS AND DISCUSSION

A. Paramagnetic state

1. NMR spectrum

For the K and $1/T_1$ measurements of $Ca_3Co_2O_6$, the external magnetic field must be adjusted precisely parallel or perpendicular to the c axis, because the magnetic susceptibility sensitively changes with the magnetic field direction around the a axis perpendicular to the chain.[17] Figure 1(a) shows the angle dependence of ^{59}Co NMR spectra was measured at 300 K, where the magnetic field direction θ is measured from the c axis, and the a^* axis is taken as the direction perpendicular to both the c and a axes. We observed a couple of sharp resonance lines arising from one Co site with the nuclear quadrupole splitting of $I=7/2$. Since the NMR signal from the magnetic Co2 site will be wiped out due to the short T_2, the observed signal is attributed to the Co1 site with $S \sim 0$. Since the NMR spectra were symmetric to the c axis and isotropic in the ab plane of the hexagonal $R\bar{3}/c$ lattice, the uniaxial rotation around the a axis gives the electric quadrupole tensor V and the Knight shift tensor K.

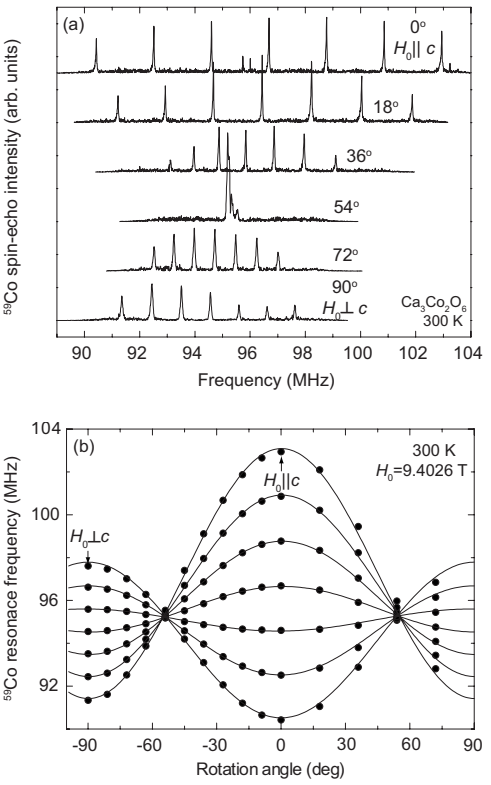

FIG. 1. (a) Angle dependence of ^{59}Co NMR spectra (Co1) of $Ca_3Co_2O_6$ at 300 K. The magnetic field H_0=9.4026 T is rotated from the c (0°) to a^* axis (90°). (b) Angle dependence of the peak positions in the ^{59}Co NMR spectra in (a).

The peak positions of the spectra in Fig. 1(a) are plotted as a function of the magnetic field direction in Fig. 1(b). Difference in the nuclear quadrupole splitting frequencies, $\delta\nu_Q$, shows a maximum value of 2.1 MHz at the c axis. $\delta\nu_Q$ decreases as the sample is rotated against H_0 and should be vanishes at the magic angle θ=54.7°, which satisfies $\delta\nu_Q = \frac{1}{84}e^2V_{ZZ}Q(3\cos^2\theta - 1) = 0$, where V_{ZZ} and eQ are the Z component of the electric field gradient tensor and the nuclear quadrupole moment, respectively. In turn, the magic angle accurately determines θ=0 as the c axis. The difference between the resonance frequencies of the $m \leftrightarrow m-1$ and $-(m-1) \leftrightarrow -m (m=-I+1, \ldots, I-1, I)$ transitions, $\nu_{m \leftrightarrow m-1}$, is generally expressed as[39]

$$\delta\nu_{m\leftrightarrow m-1} = \left(m - \frac{1}{2}\right)(k_1 + k_2 \cos 2\theta + k_3 \sin 2\theta) \quad (1)$$

in the first-order perturbation applicable to the electric quadrupole interaction much smaller than the Zeeman energy, where $k_1 = \nu_Q(V_{aa} + V_{a^*a^*})/V_{ZZ}$, $k_2 = \nu_Q(V_{aa} - V_{a^*a^*})/V_{ZZ}$, $k_3 = -2\nu_Q V_{aa^*}/V_{ZZ}$, and $\nu_Q = 3eQV_{ZZ}/2I(2I-1)h$. A fitting of the experimental data in Fig. 1(b) gives the principal components of the $\nu_Q \mathsf{V}/V_{ZZ}$ tensor as (1.04, 1.04, and 2.10 MHz) at 300 K. In general, V reflects the on-site and off-site charge distributions determined by the orbital occupancy and the distortion of the CoO_6 octahedra, respectively. In the present case, however, the on-site contribution is negligible on the Co^{3+} ion because of the fully occupied t_{2g} levels, and the off-site contribution arising from a trigonal distortion of the CoO_6 octahedron governs the anisotropy of V.

The general formula of the central line shift $\nu_{1/2\leftrightarrow -1/2}$ is given by

$$\nu_{1/2\leftrightarrow -1/2} = \nu_0[(1+K_X)\sin^2\theta\cos^2\phi + (1+K_Y)\sin^2\theta\sin^2\phi + (1+K_Z)\cos^2\theta], \quad (2)$$

where K_X, K_Y, and K_Z are the principal components of K, $\nu_0 = \gamma_n H_0/2\pi$, and ϕ is the azimuth angle.[40] A fitting of the experimental data in Fig. 1(b) by Eq. (2) with $\phi = 0$ yields $\mathsf{K} = (0.2\%, 0.2\%, 2.3\%)$ and the principal Z axis parallel to the c axis.

2. Knight shift vs magnetic susceptibility

In $Ca_3Co_2O_6$, the magnetic interaction between electron and nuclear spins at the Co1 site consists of the transferred hyperfine and classical dipole interactions from the Co2 sites. For simplicity, we neglect the hyperfine interaction with the on-site electron spins at the low-spin Co1 site. We observed no thermal variation in $\nu_Q \mathsf{V}/V_{ZZ}$, reflecting the robust crystal structure.

Figure 2 shows the temperature dependence of K in a magnetic field applied parallel and perpendicular to the c axis, respectively, denoted as K_c and K_{a^*}. For comparison, the bulk magnetic susceptibilities χ_c and χ_{a^*} are displayed in Fig. 2(b), which qualitatively agree with the results reported by Cheng *et al.*[17] Although χ_c and χ_{a^*} increase with decreasing T, K_c and K_{a^*} exhibit contrasting temperature dependence. The negative shift in K_{a^*} despite an increase in χ_{a^*} indicates a negative coupling constant at Co1 due to the dipole interaction. The fastening of T_2 wipes out the NMR signal below 70 K for $H_0 \| c$ and 130 K for $H_0 \perp c$. Here K is expressed as a sum of the T-dependent spin part K_s and the T-independent part K_0 including the chemical shift and the orbital shift, namely,

$$K = K_s + K_0 = \frac{1}{N\mu_B} A_s \chi_s + K_0, \quad (3)$$

using the coupling constant A_s, the spin susceptibility χ_s, the Avogadro's number N, and the Bohr magneton μ_B. To separate K_s and K_0, K_{a^*} and K_c are plotted versus χ_{a^*} and χ_c, respectively, in Fig. 3 with T as an implicit parameter after subtracting the core diamagnetic susceptibility $\chi_{dia} = -1.16 \times 10^{-4}$ emu/mol from χ_{a^*} and χ_c. The intercept of the vertical axis in the K-χ plots yields the T-independent $K_0 = 1.2\%$ for $H_0 \perp c$ and 1.4% for $H_0 \| c$ while the linearity gives the coupling constants $A_s^{a^*} = -8.7$ kOe/μ_B and $A_s^c = 2.0$ kOe/μ_B. The isotropic and axial parts of the coupling constant are evaluated as $A_{iso} = (2A_s^{a^*} + A_s^c)/3 = -5.1$ kOe/μ_B and $A_{ax} = (A_s^c - A_s^{a^*})/3 = 9.7$ kOe/μ_B, respectively. As shown in the inset of Fig. 3, the net hyperfine coupling A_α ($\alpha = c$ and ab) is expressed as a sum of two kinds of transferred hyperfine coupling constants, B_α and D_α, respectively, from the nearest- and next-nearest Co2 sites; namely, $A_\alpha = 2B_\alpha + 6D_\alpha$. The much longer Co1-Co2 distance (5.312 Å) for the interchain direction than that for the intrachain (2.595 Å) suggests $B_\alpha \gg D_\alpha$. Hence the strong anisotropy in the coupling tensor indicates the anisotropic spin-polarized $3d$ orbital at the Co1 site via the transferred interaction with the Co2 sites along the c axis. In a trigonal distortion, such anisotropy is expected when the Co1 a_{1g} orbital directly couples with the

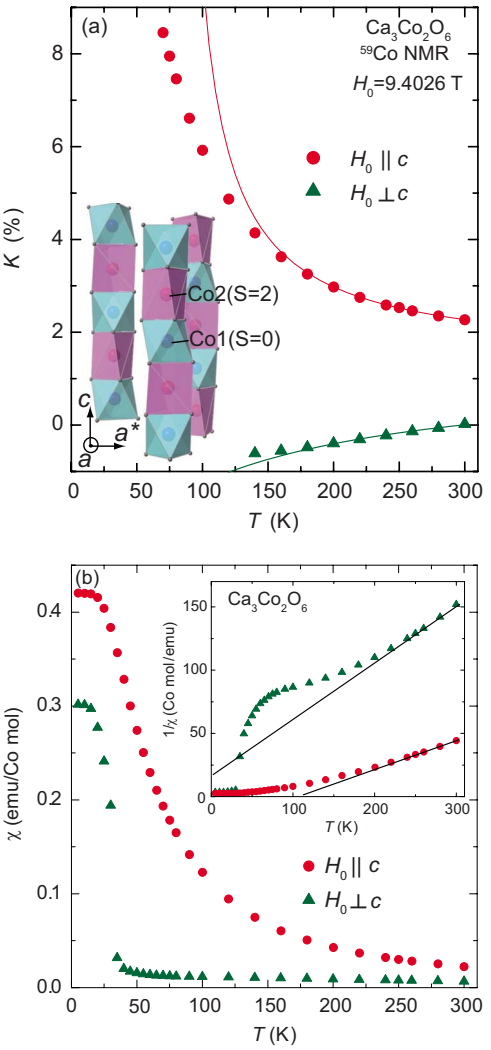

FIG. 2. (Color online) Temperature dependence of (a) ^{59}Co NMR Knight shift K and (b) magnetic susceptibility χ of $Ca_3Co_2O_6$ in a magnetic field parallel and perpendicular to the c axis. The applied magnetic field is 9.4 and 7 T for the K and χ measurements, respectively. The solid curves and lines represent the fitting results to the Curie-Weiss law in the temperature range 200–300 K.

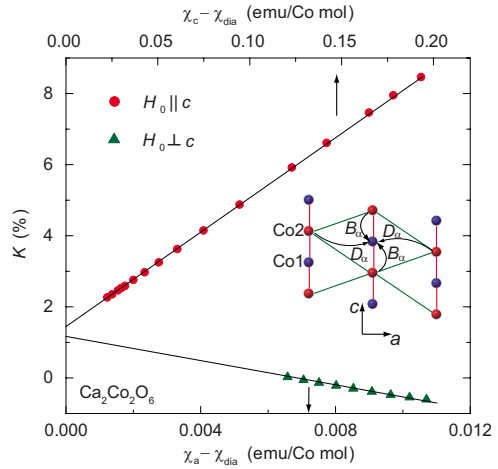

FIG. 3. (Color online) ^{59}Co Knight shift K vs magnetic susceptibility χ plots in $Ca_3Co_2O_6$ for the magnetic field parallel and perpendicular to the c axis. The transferred hyperfine coupling constants with the nearest- and next-nearest-neighbor sites, B_α and D_α, are schematically presented in the inset.

Co2 $3d_{3z^2-r^2}$ orbital, which involves the ferromagnetic interaction via the one-dimensional band.[17]

After subtracting K_0 from K, K_s is fitted to the Curie-Weiss law, $K_s = C/(T-\Theta)$, in the temperature range 200–300 K. The Weiss temperature Θ is evaluated as 77 K for $H_0 \| c$ and −90 K for $H_0 \| a^*$, indicating the intrachain ferromagnetic and interchain antiferromagnetic interactions, as seen in the previous reports.[10,17] K_s starts to deviate from the Curie-Weiss law below 140 K, as also observed in the χ^{-1}-T plot of the inset in Fig. 2(b). This is a characteristic in the low-dimensional and/or frustrated antiferromagnets exhibiting short-range correlations above T_N. Approaching to $T_N = 25$ K, χ_{a^*} shows a remarkable increase below 40 K, in contrast with the previous results measured at 0.1 T.[17] Taking into account that the magnetic field induces the fully spin-polarized state above 3.5 T, the transition at 25 K is expected to become a crossover at the present magnetic field, which may induce small ferromagnetic moments even above T_N.

3. Dynamical spin susceptibility

In presence of the nuclear quadrupole splitting, the recovery curve of the nuclear magnetization $M(t)$ after an inversion rf pulse is generally expressed by a theoretical formula for the central line of the spectrum for $I=7/2$,[41]

$$\frac{M(\infty)-M(t)}{2M(\infty)} = \frac{1}{12\,012}\{8575e^{-28t/T_1} + 2475e^{-15t/T_1} + 815e^{-6t/T_1} + 143e^{-t/T_1}\}. \quad (4)$$

Figure 4 shows the representative recovery curve measured in the magnetic field parallel to the c axis at 160 K. It is well fitted by Eq. (4) using a single fitting parameter T_1. The fitting was fairly good at all the measured temperatures in both $H_0 \| c$ and $H_0 \perp c$.

Figure 5 displays the temperature dependence of $1/T_1$ measured in the magnetic field along the a^* and c axes, respectively, denoted as $1/T_{1,a^*}$ and $1/T_{1,c}$. $1/T_{1,a^*}$ increases

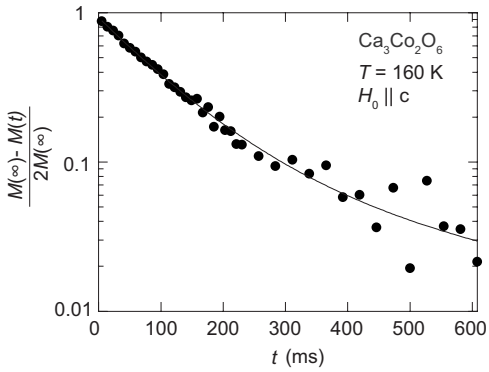

FIG. 4. ^{59}Co nuclear magnetization recovery measured for the magnetic field parallel to the c axis at 160 K. The solid curve represents the theoretical curve of Eq. (4) with $T_1 = 2.63$ ms.

monotonously upon cooling whereas $1/T_{1,c}$ decreases linearly with T at high temperatures and shows an upturn around 140 K. They are distinct from the behavior of the classical or quantum paramagnets in two- or three-dimensional lattice with the T-invariant $1/T_1$ well above T_N.[42,43]

In a paramagnetic state, $1/T_1$ is generally proportional to the wave vector $\mathbf{q}$ summation of the imaginary part of dynamical spin susceptibility $\Sigma_{\mathbf{q}}|A_\perp(\mathbf{q})|^2\chi''_\perp(\mathbf{q},\omega_n)/\omega_n$ at the nuclear Larmor frequency ω_n with the form factor $|A_\perp(\mathbf{q})|^2$ using the hyperfine coupling constant $A_\perp(\mathbf{q})$ at $\mathbf{q}$ in the plane perpendicular to the field.[42] Owing to the axially symmetric lattice of $Ca_3Co_2O_6$, $1/T_{1,a^*}$ and $1/T_{1,c}$ are simply written as

$$\frac{1}{T_{1,c}} \propto 2T\sum_q |A_{ab}(\mathbf{q})|^2 \frac{\chi''_{ab}(\mathbf{q},\omega)}{\omega}, \quad (5)$$

$$\frac{1}{T_{1,a^*}} \propto T\sum_q \left\{ |A_c(\mathbf{q})|^2 \frac{\chi''_c(\mathbf{q},\omega)}{\omega} + |A_{ab}(\mathbf{q})|^2 \frac{\chi''_{ab}(\mathbf{q},\omega)}{\omega} \right\}, \quad (6)$$

where $\chi''_\alpha(\mathbf{q},\omega)$ and $A_\alpha(\mathbf{q})$ $(\alpha = ab, c)$ are the α components of $\chi''(\mathbf{q},\omega)$ and $A(\mathbf{q})$. One can separately obtain

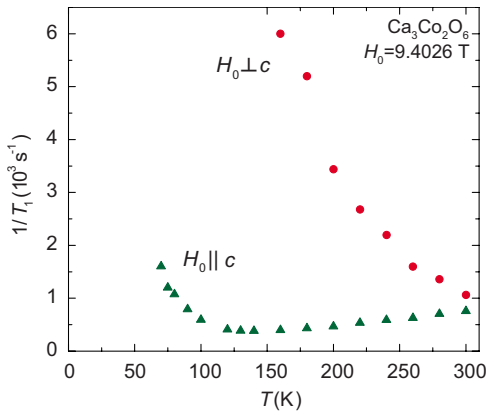

FIG. 5. (Color online) Temperature dependence of the ^{59}Co nuclear spin-lattice relaxation rate $1/T_1$ measured for the magnetic field parallel and perpendicular to the c axis in $Ca_3Co_2O_6$.

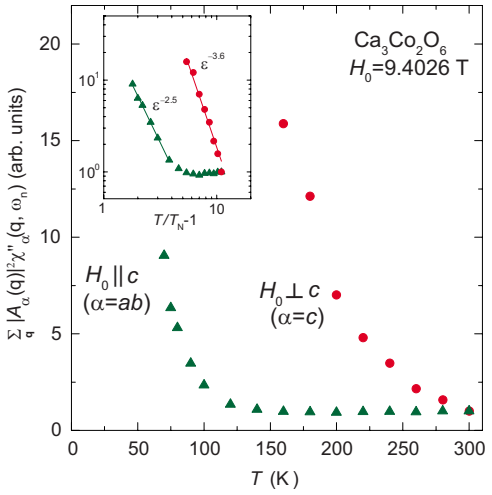

FIG. 6. (Color online) Temperature dependence of $\Sigma_{\mathbf{q}}|A_\alpha(\mathbf{q})|^2\chi''_\alpha(\mathbf{q},\omega)$, measured for the magnetic field parallel ($\alpha=c$) and perpendicular ($\alpha=ab$) to the c axis in $Ca_3Co_2O_6$. The inset shows the log plots of $\Sigma_{\mathbf{q}}|A_\alpha(\mathbf{q})|^2\chi''_\alpha(\mathbf{q},\omega)$ vs T/T_N-1.

$\Sigma_{\mathbf{q}}|A_{ab}(\mathbf{q})|^2\chi''_{ab}(\mathbf{q},\omega)$ and $\Sigma_{\mathbf{q}}|A_c(\mathbf{q})|^2\chi''_c(\mathbf{q},\omega)$ by subtracting $\frac{1}{2T_{1,c}}$ from $\frac{1}{T_{1,a}}$. Here the $\mathbf{q}$ dependence of the hyperfine coupling constant is given as $A_\alpha(\mathbf{q})=\Sigma_{\mathbf{r}}A_\alpha e^{i\mathbf{q}\cdot\mathbf{r}}\sim 2B_\alpha\cos(q_zc/4)$ for $B_\alpha \gg D_\alpha$, which is susceptible to any $\mathbf{q}$ modes except for $q_z=2\pi/c[\cos(q_zc/4)=0]$. Hence the anisotropic behavior in $\Sigma_{\mathbf{q}}|A_\alpha(\mathbf{q})|^2\chi''_\alpha$ is attributed to the anisotropy in χ''_α dominated by ferromagnetic fluctuations for $\alpha=c$ and antiferromagnetic one for $\alpha=ab$, as strongly expected from the anisotropic T dependence of K. As shown in Fig. 6, $\chi''_c(\mathbf{q},\omega)$ increases steeply from 300 K, proportional to $\sim T^{-3.6}$ as shown in the inset, while χ''_{ab} is independent of T at high temperatures above 140 K. It clearly indicates a divergent growth of ferromagnetic correlation length ξ only along the chain at high temperatures far above T_N, which constructs the paramagnetic giant Ising spins. Setting in the antiferromagnetic correlation below 120 K, as seen in an increase in χ''_{ab}, the fastening of T_2 in the ab plane ($T_2<2\times10^{-6}$ s) wipes out the NMR signal. The large $1/T_2$ despite the small A_s^{a*} and A_s^c will arise from the large χ''_α due to fluctuations of the giant spins.

The standard analysis of $1/T_1$ above T_N is a power-law fit, as expected from the dynamical scaling theory.[1] In a 2D Ising antiferromagnet, $1/T_1\sim T\Sigma_{\mathbf{q}}|A_\alpha(\mathbf{q})|^2\chi''_\alpha$ scales to ϵ^{-n} with $\epsilon=1-T_N/T$ and $n=\nu(2-\eta)=1.5$, using the critical exponent of ξ, $\nu=1$, and the Fisher's exponent $\eta=1/2$.[2] We assume that the critical slowing down already starts below 120 K in the ab plane, although the observed temperature range is much higher than T_N. The log plot of $\Sigma_{\mathbf{q}}|A_{ab}(\mathbf{q})|^2\chi''_{ab}$ in the inset of Fig. 6 shows $n=2.5-1=1.5$, in good agreement with that of the 2D Ising antiferromagnet, as also observed in the planer antiferromagnets K_2MnF_4 (Ref. 44) and Rb_2CoF_4 (Ref. 45). The exponent is much larger than that of the other models such as 2D XY, 3D Ising/XY, and Heisenberg models with $n\sim0.5-0.7$,[44] as experimentally observed in FeF_2,[46] Li_7RuO_6,[47] and $LiCrO_2$.[7] Since the dynamical scaling exponent z in $1/T_1\sim\epsilon^{d-z-2+\eta}$ is $z=4-\eta$ for the Ising ferromagnet and $z=2-\eta$ for the Ising antiferromagnet,[1,48] n for the ferromagnetic correlation along the chain is expected to have a larger value than that of the antiferromagnetic one. In this respect, $n=3.6-1=2.6$ observed in the log plot of $\Sigma_{\mathbf{q}}|A_c(\mathbf{q})|^2\chi''_c$ is consistent with the ferromagnetic critical behavior. The long-lived fluctuations below $\epsilon\sim10$, despite the divergent growth of ξ, will be ascribed to the combined effect of frustration and low dimensionality.

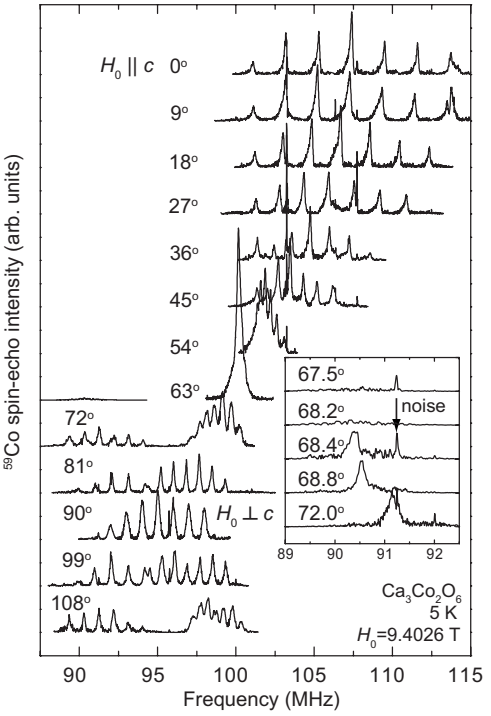

FIG. 7. Angular dependence of the ^{59}Co NMR spectra measured at 5 K and $H_0=9.4026$ T rotated in the ca^* plane for the single crystal of $Ca_3Co_2O_6$. The inset shows the spectra of the down branch in an angle range where the ferrimagnetic-ferromagnetic transition occurs.

B. Magnetically ordered state

Below 25 K, $Ca_3Co_2O_6$ undergoes the phase transition into an incommensurate magnetic order at zero field and a ferrimagnetic order below 3.5 T applied along the c axis.[10,17,29] NMR measurements on the Co1 site under the high magnetic field may have to destroy the low-field states. In this section, we present the results of NMR experiments on rotating the magnetic field which can effectively reduce the external field component along the c axis. We also show the dynamical properties in the magnetic field parallel and perpendicular to the c axis.

1. NMR spectrum

Figure 7 shows the angle dependence of the NMR spectra under $H_0=9.4023$ T rotated in the ca^* plane at 5 K. We observed sharp seven lines due to the nuclear quadrupole splitting at the magnetic field adjusted parallel to the a^* axis ($H_0\perp c$). At the field direction, the external field along the c axis vanishes. The magnetization increases linearly with $H_0\perp c$,[17] but the magnetic structure has not been known. A line broadening arising from the incommensurate magnetic

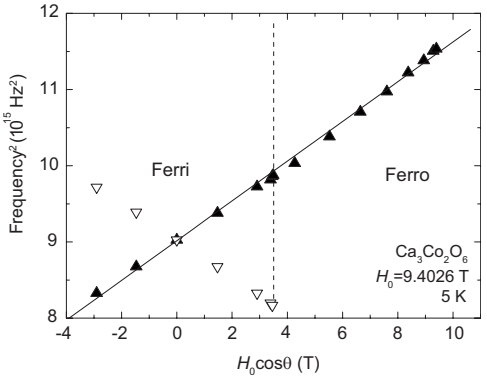

FIG. 8. The square of the central peak frequency of the ^{59}Co NMR spectra measured at 5 K and H_0=9.4023 T in Fig. 7, plotted as a function of $H_0 \cos\theta$.

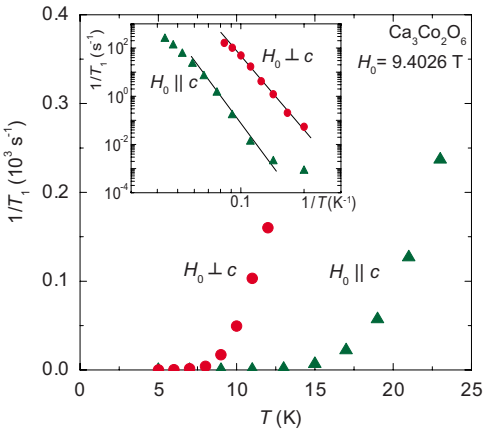

FIG. 9. (Color online) Temperature dependence of the ^{59}Co nuclear spin-lattice relaxation rate $1/T_1$ measured for $H_0 \| c$ and $H_0 \perp c$ in $Ca_3Co_2O_6$. The inset shows the activation plot of $1/T_1$ below T_N.

order is not seen in the NMR spectrum at $H_0 \perp c (H_0 \| a^*)$. Namely, the magnitude of the magnetic moment is spatially uniform. The number of resonance line doubles by tilting the external field from the a^* axis, indicating the appearance of two kinds of the local field at the Co1 sites. As seen at 72°, the high-frequency spectra have the larger intensity than that of the low-frequency spectra, which manifests the ferrimagnetic state induced by the magnetic field along the c axis. The low-frequency spectra suddenly disappear between the magnetic field direction of 68.2° and 68.4° as seen in the inset of Fig. 7. It gives microscopic evidence of the first-order transition from the ferrimagnetic to ferromagnetic state.

In the magnetically ordered state, the nuclear spins experience a sum field $\mathbf{H}$ of the internal field from the magnetic moments, $\mathbf{H}_n$, and the external field $\mathbf{H}_0$, i.e., $\mathbf{H}=\mathbf{H}_0+\mathbf{H}_n$. Thus the resonance condition is expressed as

$$\omega = \gamma_n H = \gamma_n \sqrt{H_0^2 + H_n^2 + 2H_0 H_n \cos\theta'}, \qquad (7)$$

where θ' is the angle between H_0 and H_n. We plot in Fig. 8 the square of the central resonance frequency $(\omega/2\pi)^2$ as a function of the c-axis component of the external field, $H_0 \cos\theta$. The good linearity indicates $\theta' = \theta$; namely, the magnetic moments are perfectly aligned and locked along the c axis. A ferrimagnetic-ferromagnetic transition occurs at $H_0 \cos\theta$=3.5 T projected to the c axis, in good agreement with the magnetic susceptibility on the aligned crystals.[17] The linearity in Fig. 8 yields H_n=1.2 T, which corresponds to the magnetic moment of 6 μ_B evaluated by using A_s^c =2.0 kOe/μ_B. This value is somewhat greater than 4.7 μ_B obtained from the saturated magnetization at high fields.[17] It may be attributed to underestimation of the hyperfine coupling constant in the K-χ plots in which we have neglected the on-site electron spin polarization at the Co1 site.

2. Nuclear spin-lattice relaxation rate

The NMR signal becomes detectable below 24 K for $H_0 \| c$ and 13 K for $H_0 \perp c$ due to the slowing down of T_2. The slow spin dynamics (less than approximately kilohertz), if any, would be reflected as broadening in the NMR spectra. However, no broadening of the spectra in Fig. 7 shows that the magnetic moments freeze below T_N at least at the present magnetic field. The spin dynamics can be directly observed through $1/T_1$ measurements. Even below T_N, $1/T_1$ was obtained from the same formula of the recovery curve in Eq. (1). It indicates that the nuclear spins experience nearly homogeneous local fields, as also reflected in the narrow linewidth of the NMR spectrum, ~300 kHz, as shown in Fig. 7.

Figure 9 shows the temperature dependence of $1/T_{1,c}$ and $1/T_{1,a^*}$ below T_N. Both $1/T_{1,c}$ and $1/T_{1,a^*}$ are abruptly suppressed with decreasing temperature, following the activation behavior, $1/T_1 \propto \exp(-\Delta/T)$, with a gap Δ of 154 K and 88 K for $H_0 \| c$ and $H_0 \perp c$, respectively, as shown in the inset of Fig. 9. In the antiferromagnetically ordered state, the low-lying spin excitation is usually complex but expected to be dominated by the two-magnon Raman process.[49] The exponential decay of $1/T_1$ indicates opening of a full gap in the $\mathbf{q}$ space. The angular dependence of Δ implies the anisotropic magnon dispersion. It is noted that Δ is much larger than T_N and comparable to the antiferromagnetic Weiss temperature Θ=−90 K. Since the magnitude of the magnon gap is attributed to the easy-axis single-ion anisotropy,[49] the large Δ confirms the strong Ising anisotropy in $Ca_3Co_2O_6$. The Δ relative to T_N is even greater than those of the quasi-1D antiferromagnets such as $CsCoCl_3$ (T_N=9 K, $\Delta \sim$40 K),[50] $NaVGe_2O_6$ (T_N=18 K, $\Delta \sim$12 K),[51] and $LiVGe_2O_6$ (T_N =23 K, $\Delta \sim$83 K).[52]

IV. CONCLUSION

We reported the experimental results of the detailed ^{59}Co NMR measurement first made on a single crystal of $Ca_3Co_2O_6$, the model material of the frustrated Ising triangular lattice antiferromagnet consisting of ferromagnetic S=2 chains. The angular dependence of the ^{59}Co NMR spectra arising from the nonmagnetic Co1 site provided the Knight shift and the electric field gradient tensors at 300 K, which allowed to adjusting the magnetic field accurately to the crystal axis. The temperature dependence of the ^{59}Co Knight shifts measured along a^* and c axes was well scaled to the

magnetic susceptibility and yielded the axially symmetric hyperfine coupling constants as $A_s^{a^*}=-8.7$ kOe/μ_B and $A_s^c=2.0$ kOe/μ_B. The strong anisotropy in the hyperfine coupling tensor suggests that the orbitals contributing to the transferred hyperfine coupling are axially elongated along the c axis, consistent with the ferromagnetic interaction due to the one-dimensional $3d_{3z^2-r^2}$ band. The nuclear spin-lattice relaxation rate $1/T_1$ measured along the a^* and c axes separately gave the dynamic spin susceptibility along the ferromagnetic chain and the frustrated antiferromagnetic plane in the paramagnetic state. The critical exponent for the antiferromagnetic correlation in the initial temperature range agreed with that of the 2D Ising antiferromagnet. The large anisotropic spin excitation gap compared to other Ising antiferromagnets was observed in the magnetically ordered state. These results confirmed that $Ca_3Co_2O_6$ is an ideal model of the classical 2D Ising antiferromagnet in both the paramagnetic state and the magnetically ordered state. The transverse magnetic field along the a^* axis also stabilized the ferrimagnetic state, as observed in the sharp NMR spectra. The microscopic evidence for the first-order ferrimagnetic-ferromagnetic transition was obtained at the effective magnetic field of 3.5 T applied along the c axis at 5 K.

ACKNOWLEDGMENTS

We thank S. Inoue for technical assistance. The magnetization data was collected at the Instrument Center, the Institute for Molecular Science, Japan, in technical assistance by T. Fujiwara. This work was financially supported by the Grant-in-Aid for Scientific Research (Grant No. 19340097) from the Japan Society for the Promotion of Science, and the Grant-in-Aid for Scientific Research on Priority Areas "Novel State of Matter Induced by Frustration" (Grant No. 22014006) and Special Coordination Funds for Promoting Science and Technology (SCF) from the Ministry of Education, Culture, Sports, Science and Technology, Japan.

[1] P. C. Hohenberg and B. I. Halperin, Rev. Mod. Phys. **49**, 435 (1977).
[2] C. Hohenemser, N. Rosov, and A. Kleinhammers, Hyperfine Interact. **49**, 267 (1989).
[3] H. Kawamura, J. Phys.: Condens. Matter **10**, 4707 (1998).
[4] H. Kawamura and S. Miyashita, J. Phys. Soc. Jpn. **53**, 4138 (1984).
[5] H. Kadowaki, K. Ubukoshi, K. Hirakawa, J. L. Martinez, and G. Shirane, J. Phys. Soc. Jpn. **56**, 4027 (1987).
[6] M. Heinrich, H.-A. Krug von Nidda, A. Loidl, N. Rogado, and R. J. Cava, Phys. Rev. Lett. **91**, 137601 (2003).
[7] L. K. Alexander, N. Büttgen, R. Nath, A. V. Mahajan, and A. Loidl, Phys. Rev. B **76**, 064429 (2007).
[8] R. Coldea, D. A. Tennant, E. M. Wheeler, E. Wawrzynska, D. Prabhakaran, M. Telling, K. Habicht, P. Smeibidl, and K. Kiefer, Science **327**, 177 (2010).
[9] H. Fjellvåg, E. Gulbrandsen, S. Aasland, A. Olsen, and B. C. Hauback, J. Solid State Chem. **124**, 190 (1996).
[10] H. Kageyama, K. Yoshimura, K. Kosuge, H. Mitamura, and T. Goto, J. Phys. Soc. Jpn. **66**, 1607 (1997); H. Kageyama, K. Yoshimura, K. Kosuge, M. Azuma, M. Takano, H. Mitamura, and T. Goto, *ibid.* **66**, 3996 (1997); H. Kageyama, S. Kawasaki, K. Mibu, M. Takano, K. Yoshimura, and K. Kosuge, Phys. Rev. Lett. **79**, 3258 (1997).
[11] K. E. Stitzer, J. Darriet, and H.-C. zur Loye, Curr. Opin. Solid State Mater. Sci. **5**, 535 (2001).
[12] S. Niitaka, K. Yoshimura, K. Kosuge, M. Nishi, and K. Kakurai, Phys. Rev. Lett. **87**, 177202 (2001).
[13] N. Mohapatra, K. K. Iyer, S. Rayaprol, and E. V. Sampathkumaran, Phys. Rev. B **75**, 214422 (2007).
[14] Y. J. Choi, H. T. Yi, S. Lee, Q. Huang, V. Kiryukhin, and S.-W. Cheong, Phys. Rev. Lett. **100**, 047601 (2008).
[15] T. Takami, H. Ikuta, and U. Mizutani, Jpn. J. Appl. Phys., Part 1 **43**, 8208 (2004).
[16] R. Frésard, C. Laschinger, T. Kopp, and V. Eyert, Phys. Rev. B **69**, 140405(R) (2004).
[17] J.-G. Cheng, J.-S. Zhou, and J. B. Goodenough, Phys. Rev. B **79**, 184414 (2009).
[18] H. Wu, M. W. Haverkort, Z. Hu, D. I. Khomskii, and L. H. Tjeng, Phys. Rev. Lett. **95**, 186401 (2005).
[19] V. Hardy, S. Lambert, M. R. Lees, and D. McK. Paul, Phys. Rev. B **68**, 014424 (2003).
[20] T. Goko, N. Nomura, S. Takeshita, and J. Arai, J. Magn. Magn. Mater. **272-276**, E633 (2004).
[21] S. Aasland, H. Fjellvåg, and B. Hauback, Solid State Commun. **101**, 187 (1997).
[22] O. A. Petrenko, J. Wooldridge, M. R. Lees, P. Manuel, and V. Hardy, Eur. Phys. J. B **47**, 79 (2005).
[23] M. Mekata, J. Phys. Soc. Jpn. **42**, 76 (1977).
[24] S. Agrestini, L. C. Chapon, A. Daoud-Aladine, J. Schefer, A. Gukasov, C. Mazzoli, M. R. Lees, and O. A. Petrenko, Phys. Rev. Lett. **101**, 097207 (2008).
[25] A. Bombardi, C. Mazzoli, S. Agrestini, and M. R. Lees, Phys. Rev. B **78**, 100406(R) (2008).
[26] L. C. Chapon, Phys. Rev. B **80**, 172405 (2009).
[27] U. K. Rößler, A. N. Bogdanov, and C. Pfleiderer, Nature (London) **442**, 797 (2006).
[28] A. Maignan, C. Michel, A. C. Masset, C. Martin, and B. Raveau, Eur. Phys. J. B **15**, 657 (2000).
[29] V. Hardy, M. R. Lees, O. A. Petrenko, D. McK. Paul, D. Flahaut, S. Hébert, and A. Maignan, Phys. Rev. B **70**, 064424 (2004); A. Maignan, V. Hardy, S. Hébert, M. Drillon, M. R. Lee, O. Ptrenko, D. McK. Paul, and D. Khomskii, J. Mater. Chem. **14**, 1231 (2004).
[30] X. Yao, S. Dong, H. Yu, and J. Liu, Phys. Rev. B **74**, 134421 (2006).
[31] X. Yao, S. Dong, K. Xia, P. Li, and J. M. Liu, Phys. Rev. B **76**, 024435 (2007).
[32] Y. B. Kudasov, A. S. Korshunov, V. N. Pavlov, and D. A. Maslov, Phys. Rev. B **78**, 132407 (2008).
[33] Y. B. Kudasov, Phys. Rev. Lett. **96**, 027212 (2006).
[34] V. Hardy, D. Flahaut, M. R. Lees, and O. A. Petrenko, Phys. Rev.

B **70**, 214439 (2004).
[35] T. Burnus, Z. Hu, M. W. Haverkort, J. C. Cezar, D. Flahaut, V. Hardy, A. Maignan, N. B. Brookes, A. Tanaka, H. H. Hsieh, H. J. Lin, C. T. Chen, and L. H. Tjeng, Phys. Rev. B **74**, 245111 (2006).
[36] J. Sugiyama, H. Nozaki, Y. Ikedo, K. Mukai, D. Andreica, A. Amato, J. H. Brewer, E. J. Ansaldo, G. D. Morris, T. Takami, and H. Ikuta, J. Magn. Magn. Mater. **310**, 2719 (2007); Phys. Rev. Lett. **96**, 197206 (2006).
[37] E. V. Sampathkumaran, N. Fujiwara, S. Rayaprol, P. K. Madhu, and Y. Uwatoko, Phys. Rev. B **70**, 014437 (2004).
[38] E. Woermann and A. Muan, J. Inorg. Nucl. Chem. **32**, 1455 (1970).
[39] G. M. Volkoff, Can. J. Phys. **31**, 820 (1953).
[40] C. P. Slichter, *Principles of the Magnetic Resonance*, 3rd ed. (Springer-Verlag, Berlin, 1990).
[41] A. Narath, Phys. Rev. **162**, 320 (1967).
[42] T. Moriya, J. Phys. Soc. Jpn. **18**, 516 (1963).
[43] S. Sachdev, Phys. Rev. B **50**, 13006 (1994).
[44] C. Bucci and G. Guidi, Phys. Rev. B **9**, 3053 (1974).
[45] C. Bucci and G. Guidi, J. Phys. (Paris), Colloq. **32**, C1-887 (1971).
[46] A. M. Gottlieb and P. Heller, Phys. Rev. B **3**, 3615 (1971).
[47] Y. Itoh, C. Michioka, K. Yoshimura, K. Nakajima, and H. Sato, J. Phys. Soc. Jpn. **78**, 023705 (2009).
[48] H. Benner and J. P. Boucher, in *Magnetic Properties of Layered Transition Metal Compounds*, edited by L. J. de Jonh (Kluwer Academic, Dordrecht, Boston, London, 1990), pp. 323–378.
[49] D. Hone, V. Jaccarino, T. Ngwe, and P. Pincus, Phys. Rev. **186**, 291 (1969).
[50] T. Kohmoto, T. Goto, S. Maegawa, N. Fujiwara, Y. Fukuda, M. Kunitomo, and M. Mekata, Phys. Rev. B **57**, 2936 (1998).
[51] B. Pedrini, J. L. Gavilano, D. Rau, H. R. Ott, S. M. Kazakov, J. Karpinski, and S. Wessel, Phys. Rev. B **70**, 024421 (2004).
[52] J. L. Gavilano, S. Mushkolaj, H. R. Ott, P. Millet, and F. Mila, Phys. Rev. Lett. **85**, 409 (2000).